Small-Angle X-ray Scattering and Rheological Characterization of Alginate Gels. 1. Ca−Alginate Gels

Bjørn T. Stokke,*,† Kurt I. Draget,‡ Olav Smidsrød,‡ Yoshiaki Yuguchi,§ Hiroshi Urakawa,§ and Kanji Kajiwara*,§

NOBIPOL, Department of Physics, The Norwegian University of Science and Technology, NTNU, N-7491 Trondheim, Norway, NOBIPOL, Department of Biotechnology, The Norwegian University of Science and Technology, NTNU, N-7491 Trondheim, Norway, and Faculty of Engineering and Design, Kyoto Institute of Technology, Matsugasaki, Sakyo-ku, Kyoto 606-8585, Japan

Received September 14, 1999; Revised Manuscript Received December 20, 1999

ABSTRACT: Ca−alginate gels were studied by small-angle X-ray scattering and rheology to determine relations between chemical composition and concentrations of the alginate and the elasticity and structure of the gels. The gels were prepared by in situ release of Ca^{2+} from either Ca−EGTA or $CaCO_3$ with total Ca^{2+} concentration in the range 5−30 mM. Alginates with low (39%), intermediate (50%), and high (68%) fractions of α-L-GulA originating from the brown algae *Ascophyllum nodosum*, *Laminaria hyperborea* leaf, and *Laminaria hyperborea* stipe, respectively, were employed. Two to three different degrees of polymerization for each chemical composition were used in the experiments. The excess small-angle X-ray scattering for the alginates in solution yielded linear cross-sectional Guinier plots, and the cross-sectional radius of gyration, $R_{g,c}$, was determined to be 3.1−4.6 Å. The SAXS profiles of the alginate gels depended on the alginate concentration, Ca^{2+} concentration, and the alginate composition. The SAXS data suggested that dimerization of chain segments was the principal association mode at low fractional Ca^{2+} saturation of guluronic acid of the alginate. Increasing the fractional Ca^{2+} saturation of guluronic acid, either by the concentrations or selection of alginate source, yielded coexisting lateral association modes, as manifested in a curvature in the cross-sectional plots. The coexisting junction zone multiplicities occur because of a delicate balance between the block length distribution of the α-L-GulA residues, polymer concentration, and Ca^{2+}. These results are quantitative extensions of the "egg-box" model used to describe ionotropic gelation of alginate and hence enhance the understanding of the structure−function relationship of alginate gels.

Introduction

Alginate, an unbranched copolysaccharide isolated from brown seaweeds and certain bacteria, consists of (1→4)-linked residues of β-D-ManA (M) and its C5-epimer, α-L-GulA (G). The chemical composition and sequence of the two types of residues depend on the biological source and the growth and seasonal conditions of the plants (for a recent review see ref 1). Commercially, alginate is used mainly as a gelling agent in numerous food and pharmaceutical applications. Since alginates from different sources are available, tailor-making of gel properties suitable for a given application is possible. Gel entrapment of living cells employing alginate gels is possible because the cold setting ionotropic gels are easy to make, and the correspondingly mild gelling conditions are compatible with requirements imposed by living cells. One example in this respect is the immobilization of insulin-producing Langerhans islets for subsequent human implantation for the treatment of diabetes.[2−4] In this application, the alginate gel serves as an immunobarrier excluding antigens from the gel particles and at the same time allowing nutrients and signal molecules, in particular glucose and insulin, to diffuse almost unrestricted in the gel matrix. Careful design of the gel matrix with respect to pore size and pore size distribution is necessary to achieve this.[5,6]

The "egg-box" model for ionotropic gelation of alginate describes divalent ions such as Ca^{2+}, embodied in cavities that can be formed by a cooperative pairing of contiguous G-residues.[7,8] This hypothesis is based on X-ray fiber diffraction of dehydrated specimens,[9,10] determination of the activity coefficient of Ca^{2+} in aqueous solutions of oligoguluronate with increasing degree of polymerization,[11] a highly selective binding of alkaline earth metal ions of different atomic radius,[12,13] and Ca^{2+}-induced changes in the circular dichroic spectra.[8,14] X-ray fiber diffraction of alginates enriched in G or in M showed different diffraction patterns.[7,8] On the basis of these studies, the guluronic acid was found to be in the alternate $^1C_4$ conformation, and paired G-sequences making a buckled, 2-fold structure were suggested to form cavities to accommodate divalent cations in a chelate type of binding.

In the first proposition of the "egg-box" model, the junction zones were described as microcrystallites, and hence, multiple lateral associated oligoguluronate sequences were allowed.[7] On the basis of low turbidity and low shrinkage of G-rich calcium alginate gels, the gel strength dependence on alginate concentration, and electron microscopic evidence, Smidsrød[15] later suggested that the junctions consisted of two or only a few laterally associated chain sequences. In subsequent studies by the Rees group, it was suggested that the most stable junction zones consisted of dimers.[8] This conclusion was based on equilibrium dialysis studies of Ca^{2+} binding in the presence of high concentrations of

† Department of Physics, The Norwegian University of Science and Technology.
‡ Department of Biotechnology, The Norwegian University of Science and Technology.
§ Kyoto Institute of Technology.
* Corresponding authors.

10.1021/ma991559q CCC: $19.00
Published on Web 02/18/2000

Table 1. Alginate Samples, Chemical Composition, and Intrinsic Viscosity

alginate source	F_G[a]	F_{GG}[a]	F_{MG}[a]	F_{MM}[a]	$[\eta]$ (mL/g)	$M_w/10^3$ (g mol^{-1})	sample designation
Ascophyllum nodosum	0.39	0.23	0.16	0.46	740	230	LoG_{230}
Laminaria hyperborea, leaf	0.53	0.30	0.23	0.24	500	155	InG_{155}
Laminaria hyperborea leaf	0.50	0.31	0.19	0.31	1420	455	InG_{455}
Laminaria hyperborea stipe	0.70	0.58	0.11	0.19	170	51	HiG_{51}
Laminaria hyperborea stipe	0.68	0.52	0.16	0.17	520	160	HiG_{160}
Laminaria hyperborea stipe	0.66	0.54	0.12	0.22	1440	465	HiG_{465}

[a] The symbol depicts either the fraction (one subscript) or duplet fraction (two subscripts) of the samples.

monovalent (Na^+) cations and experimentally determined changes in circular dichroism spectra as a function of the stoichiometric ratio between the divalent ions (Ca^{2+}) and the content of guluronic acid. In more recent studies a detailed localization of the Ca^{2+} ions within the paired sequences of guluronic acid residues was suggested on the basis of the molecular models consistent with the reflections observed by X-ray fiber diffraction.[16] The localization of the Ca^{2+} ions relative to the guluronic acid residues as deduced from NMR measurements[17] was not, however, clearly indicated by the X-ray fiber diffraction studies. This is in contrast to the determination of the position of ions in gellan gum based on X-ray fiber diffraction.[18,19] One reason for this could be that there is more than one possible localization of the Ca^{2+} ions that promotes lateral association, as inferred from the two possible localizations of Ca^{2+} in junction zones based on X-ray fiber diffraction.[16]

The motivation for the present study is to determine the structure of alginate gels using the small-angle X-ray scattering (SAXS) method combined with the determination of their elastic properties. SAXS affords information about the cross-sectional radius of gyration of the gels to assess the junction zone multiplicity or the size of the junction zone domains. Recently, Wang and co-workers[20] reported SAXS data obtained on gels prepared from one alginate sample by direct addition of aqueous Ca^{2+} ions over a rather limited range of low concentrations. Addition of gel-inducing ions to high-molecular-weight alginate in aqueous solution results in macroscopically inhomogeneous structures due to the rapid ion binding,[21−23] and this rapid ion binding is the basis for the use of alginate to immobilize or encapsulate enzymes or living cells. We have therefore adopted a preparation technique that employs in situ release from a Ca source, either Ca−EGTA or $CaCO_3$, to obtain homogeneous gels. By this preparative technique, different amounts of calcium ions may be introduced to achieve various stoichiometric ratios between Ca^{2+} and G-residues of the alginate while at the same time avoiding problems associated with macroscopic concentration gradients. The structural studies on a local scale using SAXS are supplemented with rheological determination of the gelation process and of the final gels. This is carried out using well-characterized alginate samples from three different sources. Compared to the study by Wang and co-workers,[20] the present investigation also spans a broader range of Ca^{2+} and alginate concentrations and uses different alginate sources with respect to chemical composition and chain length.

Materials and Methods

Alginate Samples. Alginate samples isolated from various sources were kindly provided by Pronova Biopolymer a.s., Drammen, Norway. The chemical composition, the fraction of diad sequences F_{GG}, F_{MG}, and F_{MM}, determined by high field ^{1}H NMR according to Grasdalen,[24] and intrinsic viscosity, $[\eta]$, in 0.1 M NaCl at $T = 20$ °C determined in a capillary viscometer are summarized in Table 1. The ^{1}H NMR spectra showed no significant peaks originating from proteins or other impurities. The chemical composition and sequence depending of the selected alginates depended on the type of brown seaweed (Table 1) similar to that reported previously (see Moe and co-workers[1] for a recent review). A three-letter acronym was selected to depict the sample with low F_G, LoG, intermediate F_G, InG, and highest F_G, HiG (Table 1). The subscripts added to these sample designations reflect the M_w (in 10^3 g/mol) of these samples using the experimental determined $[\eta]$ and the Mark−Houwink equation $[\eta]$ (mL/g) $= 4.85 \times 10^{-3} M_w^{0.97}$ (ref 25). Alginate stock solutions with polymer concentration $c_p = 20$ mg/mL were prepared by dissolving 1.0 g in 50 mL of distilled water and stirring overnight. The resulting alginate solutions were subsequently filtered using filters with pore sizes 1.2 and 0.7 μm (Millipore). The samples were generally found to be easy to filter; therefore, the loss of polymer during the filtration was considered negligible, and no corrections in polymer concentrations were employed.

Preparation of Ca−Alginate Gels. Homogeneous Ca−alginate gels were prepared by blending the alginate stock solutions with solutions of an inactivated form of Ca^{2+} followed by addition of the slowly hydrolyzing D-glucono-δ-lactone (GDL). Both Ca^{2+} complexed with EGTA and Ca^{2+} in the form of an insoluble salt ($CaCO_3$)[26] were utilized. Ca−alginate gels were prepared by blending an appropriate volume of the 20 mg/mL alginate stock solution with the appropriate volume of a 100 mM CaEGTA solution, pH 7, followed by addition of the required amount (solid) of GDL freshly dispersed in 0.2 mL of H_2O. Finally, the total volume was adjusted to give the desired c_p and $[Ca^{2+}]$. The 100 mM CaEGTA, pH 7, stock solution was prepared by adding 3.80 g of EGTA and 1.47 g of $CaCl_2 \cdot 2H_2O$ to 50 mL of deionized H_2O, the pH was adjusted to 7 with 1 M NaOH, and the total volume finally adjusted to 100 mL. The concentration of GDL required for each concentration of Ca^{2+} when using Ca−EGTA as the Ca^{2+} source was calibrated to yield pH 4 after equilibration for about 24 h after addition of GDL. The rate of change in pH and the release of Ca^{2+} from CaEGTA were determined using a conventional pH electrode and a Ca^{2+}-sensitive electrode in parallel experiments without alginate. The gelling solutions were degassed prior to loading the samples in the sample cells for small-angle X-ray scattering experiments.

Rheological Characterization. Dynamic viscoelastic characterization of the alginate samples prior to gelation and 24 h after inducing the gelation was carried out by determining the frequency dependence of the storage and loss moduli, $G'(\omega)$ and $G''(\omega)$ at $T = 20$ °C, using a Bohlin VOR general purpose rheometer (Lund, Sweden) or a Rheologica Stresstech controlled stress rheometer (Lund, Sweden). The Bohlin VOR was employed with serrated plate−plate sample cell and torsion bar with stiffness of 4 g cm for the measurements. The samples were sealed with a low-density, low-viscosity silicon oil to avoid adverse effects associated with evaporation of solvent throughout the gelation experiments. The kinetics of gelation were determined by repeated determination of G' and G'' at $\omega = 6.28$ rad s^{-1} at $T = 20$ °C at intervals of 3 min.

Determination of Syneresis. Syneresis of the Ca−alginate gels was determined as the volume reduction of the gels. Aliquots of Ca−alginate gelling solutions prepared as described above were cured in tissue culture plates with 24 wells having

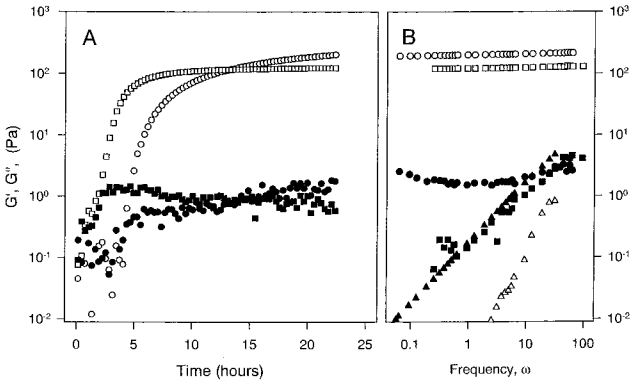

Figure 1. (A) Storage (open symbols) and loss (filled symbols) moduli at $\omega = 6.28$ rad s^{-1} at $T = 20$ °C versus time after inducing gelation by adding GDL to 10 mg/mL alginate InG_{155} solutions containing $[Ca^{2+}] = 10$ mM from Ca−EGTA (○, ●) and from $CaCO_3$ (□, ■). (B) Storage (open symbols) and loss (filled symbols) moduli versus frequency, $T = 20$ °C, for 10 mg/mL alginate LoG_{230} solution (△, ▲) and InG_{155} gels with $[Ca^{2+}] = 10$ mM from CaEGTA (○, ●) and from $CaCO_3$ (□, ■). The mechanical spectra of the gels were obtained 24 h after inducing gelation.

a diameter of 16 mm and height of 18 mm (Costar, Cambridge, MA). The gels were taken out from the wells at selected intervals and blotted off, and their dimensions were determined. The syneresis was calculated as $(1 - V/V_0) \times 100\%$, where V and V_0 are the actual and reference volume of the gel cylinders.

Small-Angle X-ray Scattering. Small-angle X-ray scattering experiments were performed employing the SAXES optics installed at the BL10-C beamline at the Photon Factory, Tsukuba, Japan.[27] A monochromatic X-ray with $\lambda = 1.488$ Å was obtained using a double-crystal monochromator of the incident X-ray from the synchrotron. This beam was focused to the cell position with the aid of a bent focusing mirror. The intensity of the scattered X-rays from the gels was determined using a one-dimensional position-sensitive proportional counter (PSPC) of an effective length of 160 mm. The PSPC was positioned at a distance 1900 mm from the specimen cuvette, yielding a scattering vector in the range $q = 0.014-0.4$ Å^{-1}. The exact distance between the sample and the camera was calibrated by the diffraction peaks of collagen as previously described.[28] The alginate gels were cured for 20−24 h in samples cells consisting of Perspex with entrance and exit windows made of mica. An integration time of 20 min was employed to obtain a good signal-to-noise ratio in the SAXS data from the gels. The excess scattering was taken as the difference between each gel and its solvent in the same sample cells. The scattered intensities were corrected with respect to the estimated X-ray absorption by determination of the transmission by inserting a standard polyethylene block with an attenuator. In the present paper, only the values at apparent equilibrium from the rheological data (i.e., after curing the gels for 24 h) are presented. Data for time-resolved small-angle X-ray scattering during gel curing will be presented elsewhere.[29]

Results and Discussion

Rheology. Figure 1a shows examples of the storage, G', and loss modulus, G'', as a function of time after inducing gelation at 20 °C of the alginate gels. Figure 1b shows examples of the frequency dependence of G' and G'' prior to and after gelation of the alginate samples. These determinations were carried out at ratios between alginate and total concentration of Ca^{2+} ions ($[Ca^{2+}]$) corresponding to nonsyneretic conditions. The data show that there is an increase of at least 2 orders of magnitude in G' associated with the gelation, whereas the change in G'' is almost negligible. The

Table 2. Storage, G', and Loss, G'', Modulus at $\omega = 6.28$ rad s^{-1} of Ca−Alginate Gels at Initiation of Gelation and after 24 h Gelation

				initial		24 h gels	
sample	c_p (g/L)	$[Ca^{2+}]$ (mM)	Ca source	G' (Pa)	G'' (Pa)	G' (Pa)	G'' (Pa)
LoG_{230}	10	10	CaEGTA	0.02	0.30	164	1.46
	10	20	CaEGTA	0.06	0.4	880	25
InG_{155}	10	10	CaEGTA	0.10	0.10	204	1.9
	10	20	CaEGTA	0.11	0.13	1200	27.9
	5	7.5	$CaCO_3$	0.06	0.11	34	0.9
	5	15	$CaCO_3$	0.15	0.14	1005	58
	10	10	$CaCO_3$	0.27	0.36	124	0.7
	10	15	$CaCO_3$	0.10	0.36	430	19.4
	10	25	$CaCO_3$	0.25	0.26	1880	116
	12.5	17.5	$CaCO_3$	0.07	0.29	247	10.6
	15	15	$CaCO_3$	0.20	0.32	283	5.6
InG_{455}	10	10	CaEGTA	0.33	1.43	833	16.9
	10	20	CaEGTA	0.20	1.80	2580	24.6
HiG_{51}	10	10	CaEGTA	0.04	0.1	280	18
	10	20	CaEGTA	0.04	0.3	2100	150
HiG_{160}	10	10	CaEGTA	0.34	0.11	800	23.5
	10	20	CaEGTA	0.15	0.33	4540	89.1
	10	10	$CaCO_3$	0.18	0.16	188	3.0
HiG_{465}	10	10	CaEGTA	0.27	2.03	1310	25.3
	10	20	CaEGTA	0.80	2.53	6120	40.5

gelation kinetics are characterized by only small changes in G' during the first 60 min, followed by a sharp increase in G' and subsequent leveling off after about 5 h. These trends were observed for all the samples for both types of Ca^{2+} sources used (Ca−EGTA or $CaCO_3$). The time before the onset of the increase in G' when using Ca−EGTA as the Ca source correlates with the time needed to reduce the pH to about 5 where the release of Ca^{2+} ions was observed in parallel experiments without alginate. The plateau value of G' depends on the alginate source and $[Ca^{2+}]$ by showing an increasing value for increasing F_G of the alginate for a given $[Ca^{2+}]$. The rheological data obtained using $CaCO_3$ as the Ca source for gelation of the InG_{155} alginate indicate that the fractional Ca saturation combined with the total polymer concentration determines the final G' (Table 2).

These observations are analogous to the previous report,[30] confirming the empirical correlation between the gel strength and the fraction of the diad F_{GG} in the sample. The present data (Table 2) also show an increase in G' of the 24 h cured gels with increasing $[Ca^{2+}]$ for a given alginate sample. This is consistent with previous observations on Ca-limited alginate gels.[31] Furthermore, the data show that the final gel strength also depends on whether Ca−EGTA or $CaCO_3$ was used as the Ca source. A difference in final pH of the gels using these two Ca sources may be one factor contributing to this difference.

The frequency dependence of G' and G'' for the alginate solution (Figure 1b) is characteristic of a viscoelastic liquid with G' being less than G'' for the lowest frequencies in the experimental range of ω and with $\log(G')$ vs $\log(\omega)$ and $\log(G'')$ vs $\log(\omega)$ having slopes of ∼2 and ∼1, respectively. The mechanical spectra of the gels (Figure 1b) show that G' is generally larger than G'' over the entire range of ω. Moreover, G' is nearly independent of the frequency in this range, indicating that an apparent steady-state situation is achieved and that the alginate gels prepared by the current method for in situ release of Ca^{2+} ions obey the criteria for being a gel.[32] The effect of kinetics of Ca^{2+} binding to alginates and alginate mobility on the concentration profiles

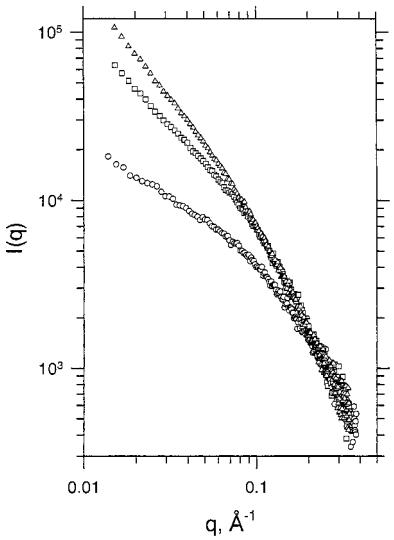

Figure 2. Small-angle X-ray scattering profiles, $I(q)$ versus q, for 10 mg/mL alginate InG_{155} in 0.1 M NaCl solution (○) and homogeneous gels at $[Ca^{2+}] = 10$ (□) and 20 mM (△), respectively, using CaEGTA as the Ca^{2+} source.

Table 3. Syneresis of 10 mg/mL InG_{155} and HiG_{160} Alginate Gels at $T = 20$ °C

sample	c_p (g/L)	$[Ca^{2+}]$ (mM)	Ca source	% syneresis at 24 h
InG_{155}	10	20	CaEGTA	7.2
	10	20	$CaCO_3$	13
	10	30	CaEGTA	8.6
	10	30	$CaCO_3$	21.6
HiG_{160}	10	20	CaEGTA	2.1
	10	20	$CaCO_3$	12.4
	10	30	CaEGTA	7.2
	10	30	$CaCO_3$	21.6

across the resulting gels have been reported.[33,34] The procedure to prepare gels for the SAXS studies was selected to yield macroscopic homogeneous concentration of the gels, thereby limiting eventual effects of the kinetics of gel formation on the gel structure.

Syneresis. The syneresis behavior was carried for $c_p = 10$ mg/ml of the InG_{155} and HiG_{160} alginates. The data for the InG_{155} sample (Table 3) show that, by using CaEGTA at $[Ca^{2+}] = 20$ mM, the syneresis is less than about 7% at 24 h after onset of gelation. Furthermore, the syneresis at $[Ca^{2+}] = 20$ mM is less pronounced when using Ca−EGTA as the Ca source compared to $CaCO_3$. The syneresis increases, and the difference between the Ca sources becomes larger when increasing the $[Ca^{2+}]$ to 30 mM. The trends as a function of $[Ca^{2+}]$ in the syneresis behavior for the HiG_{160} sample are analogous to that determined for the InG_{155} sample, but the syneresis is generally less.

Small-Angle X-ray Scattering. The excess small-angle X-ray scattering of the homogeneous alginate gels depends on the source of the alginate and $[Ca^{2+}]$, but to a lesser extent on the degree of polymerization of the polysaccharide chains. Figure 2 shows the SAXS data for 10 mg/mL LoG_{230} in solution and gels at 10 and 20 mM Ca^{2+} using Ca−EGTA. Compared to the solution, the data show a marked Ca^{2+} dependence in the scattered intensity ($I(q)$) for a scattering vector up to $q = 0.08$ Å^{-1}, with the largest changes being at the smallest accessible q.

Multiplicity of junction zones is most prominent when the Guinier approximation for the analysis of cross section is adopted. For rigid cylinders where the cross-sectional radius is much less than the length of the cylinders, the cross-sectional radius of gyration $R_{g,c}$ can be evaluated according to[35]

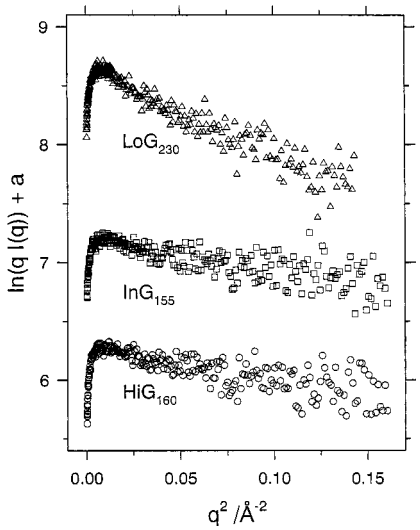

Figure 3. Cross-sectional Guinier plots of SAXS data from 10 mg/mL alginate LoG_{230} (△), InG_{155} (□), and HiG_{160} (○) in 0.1 M NaCl aqueous solutions without added Ca ions. Parameter a is an arbitrary shift factor used to distinguish between the data.

$$qI(q) \approx \exp(-R_{g,c}^{\ 2}\, q^2/2) \qquad (1)$$

Figure 3 shows the cross-sectional Guinier plots for 10 mg/mL LoG_{230}, InG_{155}, and HiG_{160} alginates in aqueous 0.1 M NaCl solutions. An analysis of the data according to eq 1 confirms that the non-cross-linked alginates assume a (locally) stiff, rodlike geometry, and the estimated $R_{g,c}$ are 4.6, 3.5, and 3.1 Å for LoG_{230}, InG_{155}, and HiG_{160}, respectively. We have observed a similar variation in the estimates of $R_{g,c}$ for several alginate oligomers derived from these sources.[36] The correlation between $R_{g,c}$ and the chemical composition of the alginate will be discussed more quantitatively later using well-defined alginate oligomers.[36]

The cross-sectional Guinier plots of $c_p = 10$ mg/mL alginate gels from the same samples at $[Ca^{2+}] = 10$ and 20 mM using CaEGTA are shown in Figure 4a. The SAXS data deviate from those expected for a one-component rodlike model by showing an up-turn curvature at low q in most cases. In the case of the sample LoG_{230} at $[Ca^{2+}] = 10$ mM, where the cross-sectional Guinier plot is nearly linear, the $R_{g,c}$ was estimated to 7.6 Å based on $q^2 \in 0.005-0.025$ Å^{-2}. This increase in $R_{g,c}$ above that for the dispersed chains associated with the gelation corresponds to junction zones being formed by a lateral condensation yielding duplex or triplex associated chain segments. Previously reported evidence showing the strong selectivity for the binding of Ca^{2+} ions to guluronic-rich alginate samples[8,12,13] argues for the guluronic sequences being paired up on gelation.

Increasing the concentration of Ca^{2+} ions to 20 mM for the LoG_{230} sample clearly yields an up-turn curvature in the low-q region of the cross-sectional Guinier plots, indicating coexisting junction zone multiplicities. An estimate $R_{g,c}$ of 9.3 Å was obtained in the limiting case for this sample, but this estimate is to a larger extent influenced by the selected range of q^2 than at $[Ca^{2+}] = 10$ mM. These trends are even more pronounced for the 10 mg/mL alginate InG_{155} and HiG_{160}

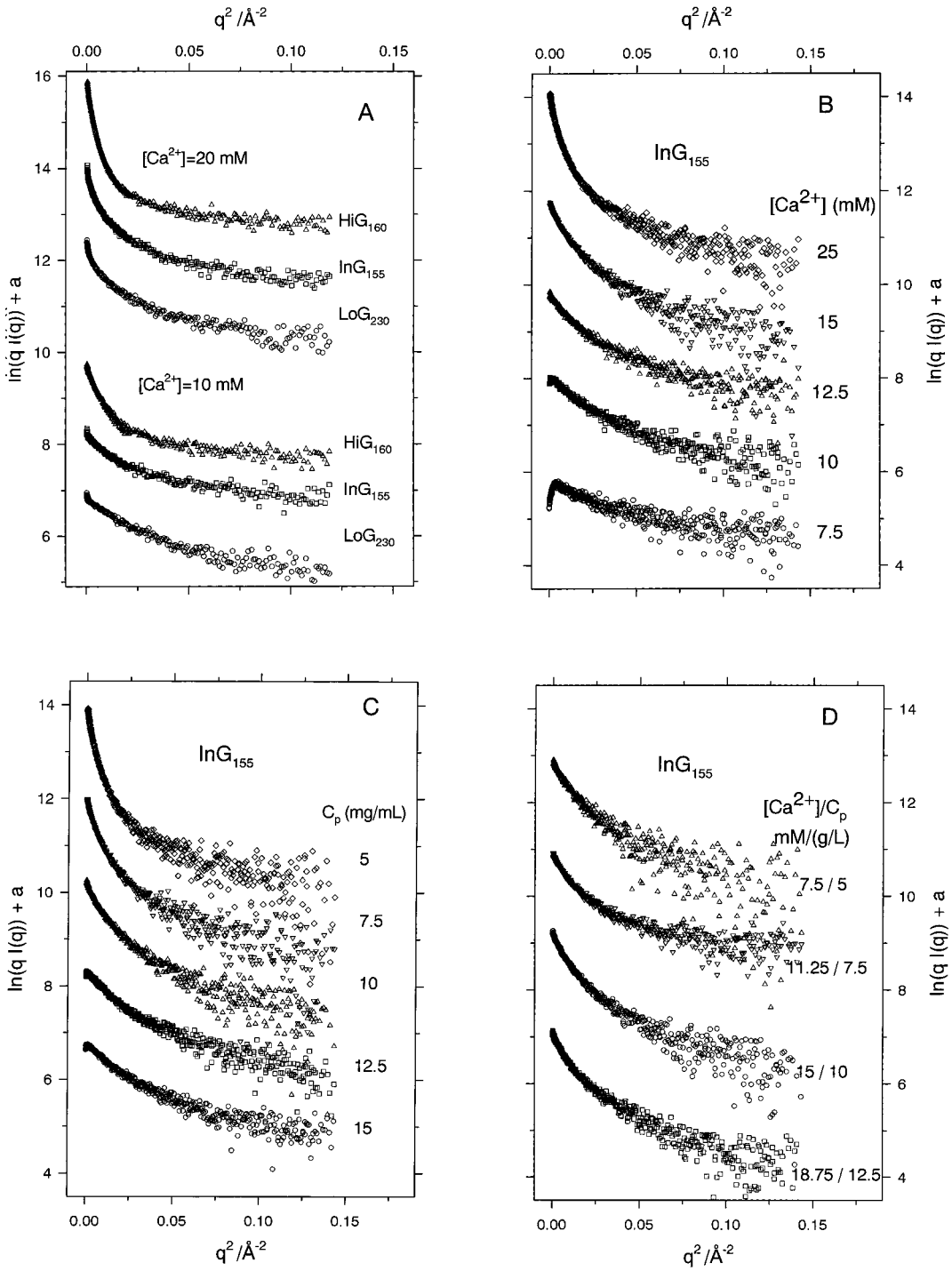

Figure 4. Cross-sectional Guinier plots of SAXS data from 10 mg/mL homogeneous alginate gels. (A) Dependence of chemical composition of the alginate sources at $[Ca^{2+}] = 10$ and 20 mM, using CaEGTA as the Ca^{2+} source. The data were obtained for alginate using alginates LoG_{230}, InG_{155}, and HiG_{160} as indicated. (B) Effect of $[Ca^{2+}]$ from 7.5 to 25 mM using $CaCO_3$ as the Ca^{2+} source on 10 mg/mL InG_{155} alginate gels. (C) Effect of alginate concentration c_p in alginate InG_{155} gels at constant $[Ca^{2+}] = 15$ mM using $CaCO_3$ as the Ca^{2+} source. (D) Cross-sectional plots of SAXS data from alginate InG_{155} gels at constant ratio between polymer concentration c_p and $[Ca^{2+}]$ concentration using $CaCO_3$ as the Ca^{2+} source. Parameter a is an arbitrary shift factor used to distinguish between the data.

gels (Figure 4a). In particular for the gels made from the HiG_{160} sample, the curvatures are too large at the shown Ca levels to estimate any limiting values of $R_{g,c}$. Further analyses of these data follow.

Figure 4b shows the cross-sectional Guinier plots of SAXS data for $c_p = 10$ mg/mL InG_{155} alginate gels for $[Ca^{2+}]$ from 7.5 to 25 mM using $CaCO_3$ as the Ca^{2+} source. These data confirm the validity of eq 1 for the lowest $[Ca^{2+}]$, whereas increasing $[Ca^{2+}]$ yields an increasing curvature in the cross-sectional Guinier plots. The cross-sectional radius of gyration $R_{g,c}$ was estimated to be 5.9 and 7.3 Å at $[Ca^{2+}] = 7.5$ and 10 mM, respectively. These data show that the lateral condensation into junction zones is not limited to one association mode, possibly by molecular details in the packing geometry, but is controlled by the concentration of Ca^{2+} for a given c_p and alginate type. To explore this further, experiments were carried out for constant $[Ca^{2+}]$ and

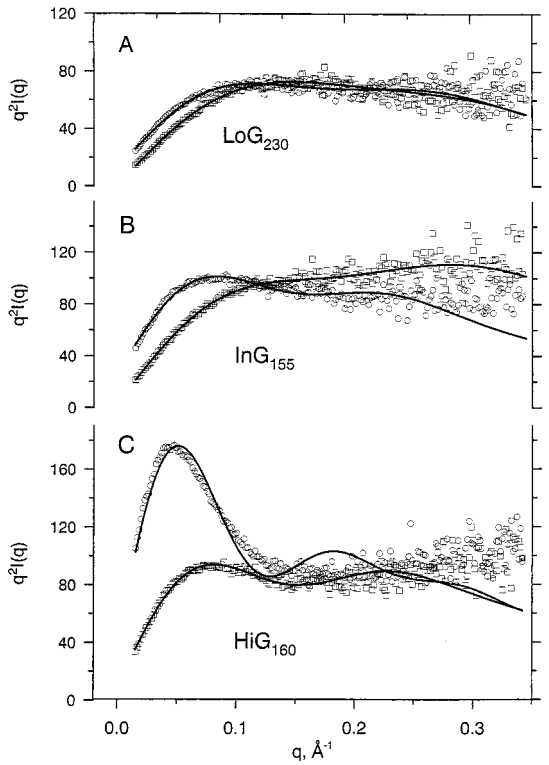

Figure 5. Kratky plots of SAXS from 10 mg/mL alginate LoG_{230} (a), InG_{155}(b), and HiG_{160} (c) gels at $[Ca^{2+}] = 10$ mM (○) and 20 mM (□), respectively, using CaEGTA as the Ca^{2+} source. The continuous lines depict the model fit to the data (see text).

increasing alginate concentration (Figure 4c) and constant ratio $[Ca^{2+}]/c_p$ for increasing c_p (Figure 4d) for the InG_{155} sample. Comparison of the cross-sectional Guinier plots obtained for the constant c_p, increasing $[Ca^{2+}]$ series with that for the increasing c_p, constant $[Ca^{2+}]$ series (Figure 4b,c) indicates that the ratio $[Ca^{2+}]/c_p$ to a large extent determines the distribution of junction zones multiplicity. The close similarity in the profile of the cross-sectional Guinier plots in Figure 4d confirmed this for one selected ratio $[Ca^{2+}]/c_p$ for the InG_{155} sample covering a 3-fold range in c_p.

More detailed information can be obtained by fitting a model to the data. Initial trials showed that a model consisting of a Gaussian chain represented by a correlation length and one rigid cylinder representing the junction zones could not adequately account for the scattering data. Thus, the broken-rod-like model allowing for polydispersity in the cross section of the junction zones represented by a two-component model was applied:[37]

$$q^2I(q) = k_1 q \frac{J_1^2(qR_1)}{qR_1} + k_2 q \frac{J_1^2(qR_2)}{qR_2} + k_3 \qquad (2)$$

In eq 2, k_1 and k_2 are the relative weights of the two rodlike components representing the junction zones, R_1 and R_2 are their radii, k_3 is an adjustable constant, and $J_1(x)$ is the first-order Bessel function. The long-range random nature of the polymer chain contributes to k_3. This model was generally found to possess sufficient flexibility to account for the experimental data. The examples of fit for $c_p = 10$ mg/mL LoG_{230}, InG_{155}, and HiG_{160} alginate gels, each at $[Ca^{2+}] = 10$ and 20 mM using CaEGTA, are shown in Figure 5. The estimated

Table 4. Cross-Sectional Radius and Weight Fraction of Broken-Rod-like Model Fit to Ca−Alginate Gels Using CaEGTA as the Ca^{2+} Source

sample	c_p (g/L)	$[Ca^{2+}]$ (mM)	R_1 (Å)	R_2 (Å)	k_1	k_2	k_3
LoG_{230}	10	10	6.2	15.4	1967	1612	0.5
	10	20	6.4	18.4	1703	2067	11.9
InG_{155}	10	10	5.1	17.0	2572	2369	2.87
	10	20	7.4	21.9	2173	4008	26.3
InG_{455}	5	5	5.0	17.4	1659	1377	2.2
	5	10	6.3	20.7	1268	2562	11.1
	10	10	5.7	15.2	2271	2738	9.4
	10	20	7.5	21.5	2709	5294	31.5
HiG_{51}	10	10	9.0	26.0	2269	6438	12.0
	10	20	10.2	33.8	676	15241	35
HiG_{160}	10	10	6.3	22.2	2302	4975	8.2
	10	20	7.4	28.8	1857	15922	38
	10	30	22.2	38.1	3973	10450	30
HiG_{465}	5	5	3.4	17.3	1323	1490	0.4
	5	10	6.7	22.4	1343	4185	10.5
	10	10	5.4	18.8	2854	3363	5.6
	10	20	7.0	24.2	2191	9522	32

Table 5. Cross-Sectional Radius and Weight Fraction of Broken-Rod-like Model Fit to Ca−Alginate Gels Using $CaCO_3$ as the Ca^{2+} Source

alginate source	c_p (g/L)	$[Ca^{2+}]$ (mM)	R_1 (Å)	R_2 (Å)	k_1	k_2	k_3
LoG_{230}	10	10	5.4	14.2	955	1323	0.7
InG_{155}	5	7.5	9.1	20.0	1109	1042	0.8
	5	15	10.6	25.2	1390	6172	10
	7.5	11.25	6.9	18.8	1588	1937	1.4
	7.5	15	10.4	23.3	1978	3302	8.0
	10	7.5	7.4		1241		0
	10	10	7.3	16.1	1668	1043	0
	10	12.5	7.3	17.8	1741	1685	0.6
	10	15	8.6	19.5	2019	2644	4.2
	10	25	9.8	23.8	1972	6564	14
	12.5	15	7.0	16.8	1868	1741	0
	12.5	18.5	8.6	20.2	1987	2221	2.9
	15	15	6.9	16.2	1963	1513	0
InG_{455}	10	10	4.7	10.9	756	1747	0
HiG_{160}	10	10	7.3	17.3	1586	1690	0
	10	30	8.2	23.8	1178	12687	20
HiG_{465}	10	10	5.0	13.6	1199	1495	0

model parameters (Tables 4 and 5) show dominant cross-sectional radii that depend on the chemical composition and $[Ca^{2+}]$. For the LoG_{230} sample using CaEGTA as the Ca^{2+} source, the model parameters show that R_1 is nearly independent of $[Ca^{2+}]$ whereas R_2 increases from 15.4 Å at $[Ca^{2+}] = 10$ mM to 18.4 Å at $[Ca^{2+}] = 20$ mM and that the relative fraction of the largest component increases. Even for this sample at $[Ca^{2+}] = 10$ mM, there is a significant fraction of the larger component although the cross-sectional plots apparently validated the use of eq 1 to fit the data. Similar trends of relatively constant R_1, increasing R_2, and increasing ratio k_2/k_1 associated with increasing $[Ca^{2+}]$ are found within each of the alginate samples (Tables 4 and 5). Comparing different alginates at a given $[Ca^{2+}]$ shows that increasing F_G of the sample generally increases R_2 and/or the ratio k_2/k_1 whereas the value of R_1 is affected to a lesser extent. The HiG_{51} sample deviates from this general trend, indicating that the degree of polymerization also affects the gel ultrastructure.

The estimated model parameters for the InG_{155} sample at constant $[Ca^{2+}]/c_p$ (Table 5) confirm the above conclusion that constant $[Ca^{2+}]/c_p$ yields a similar distribution of junction zone multiplicity at different c_p (Figure 4d). The actual values of the parameters R_1, R_2 and ratio k_2/k_1 are not identical for this constant $[Ca^{2+}]/$

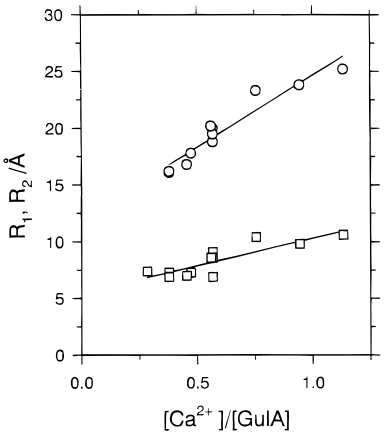

Figure 6. Cross-sectional radius, R_1 and R_2, of cylinders in the broken-rod-like model fit to the data versus stoichiometric ratio between Ca^{2+} and alginate concentration for alginate InG_{155}, using $CaCO_3$ as the Ca^{2+} source.

c_p series but are considered sufficiently similar to support that conclusion. Figure 6 shows the two parameters R_1 and R_2 versus the ratio $[Ca^{2+}]/c_p$ for all the experiments for the InG_{155} gels using $CaCO_3$ as the Ca source. The data show a good correlation between the two radii and $[Ca^{2+}]/c_p$ for these experiments. Attempts to construct a master plot of R_1 and R_2 across the alginate samples, e.g., based on fractional Ca saturation of guluronic acid, did not succeed in yielding a similar unique correlation. The estimated R_2 are 2−3 times the value of R_1. One clear trend across the samples is the relative increase of the weight fraction of the second component associated with the increase in $[Ca^{2+}]$ from 10 to 20 mM. Whether the mechanism for this is elongation of already thick junction zones or formation of new junction zones with larger dimensions by lateral association cannot be discerned from the present data.

A further aspect of the Kratky plots (Figure 5) is that the ratio between the maximum in $q^2I(q)$ to the plateau value at larger q is most pronounced for $[Ca^{2+}] = 20$ mM and the lowest degree of polymerization. This ratio reflects the number of units extending from the junction zones.[38] For the HiG sample, this is consistent with decreasing k_1/k_2 the lower the degree of polymerization in the analysis using the broken-rod-like model (Table 4). The maximum in the Kratky plots at $[Ca^{2+}] = 20$ mM increases from $q = 0.036 \pm 0.003$ Å^{-1} for the HiG_{51} (not shown) to $q = 0.043 \pm 0.004$ Å^{-1} and $q = 0.058 \pm 0.002$ Å^{-1} for the HiG_{160} and HiG_{465} samples, respectively.

Calculation of Scattering Profiles from the Molecular Model. The estimated values of R_1 in the broken-rod-like model have dimensions that exceed dispersed alginate chains as expected from the dimensions determined from X-ray fiber diffraction.[9,10] More direct comparison to the expected $R_{g,c}$ based on data reported from X-ray fiber diffraction was obtained by calculating the scattering profiles of the model junction zones based on the reported atomic coordinates.[9,10] The particle scattering factor $\Theta(q)$ was calculated as a function of q from the atomic coordinates of the model junction zones using the Debye formula:[39]

$$\Theta(q) = \sum_i g_i^2 \phi_i^2(q) + 2\sum_i \sum_j g_i g_j \phi_i(q) \phi_j(q) \frac{\sin(d_{ij}q)}{d_{ij}q} \quad (3)$$

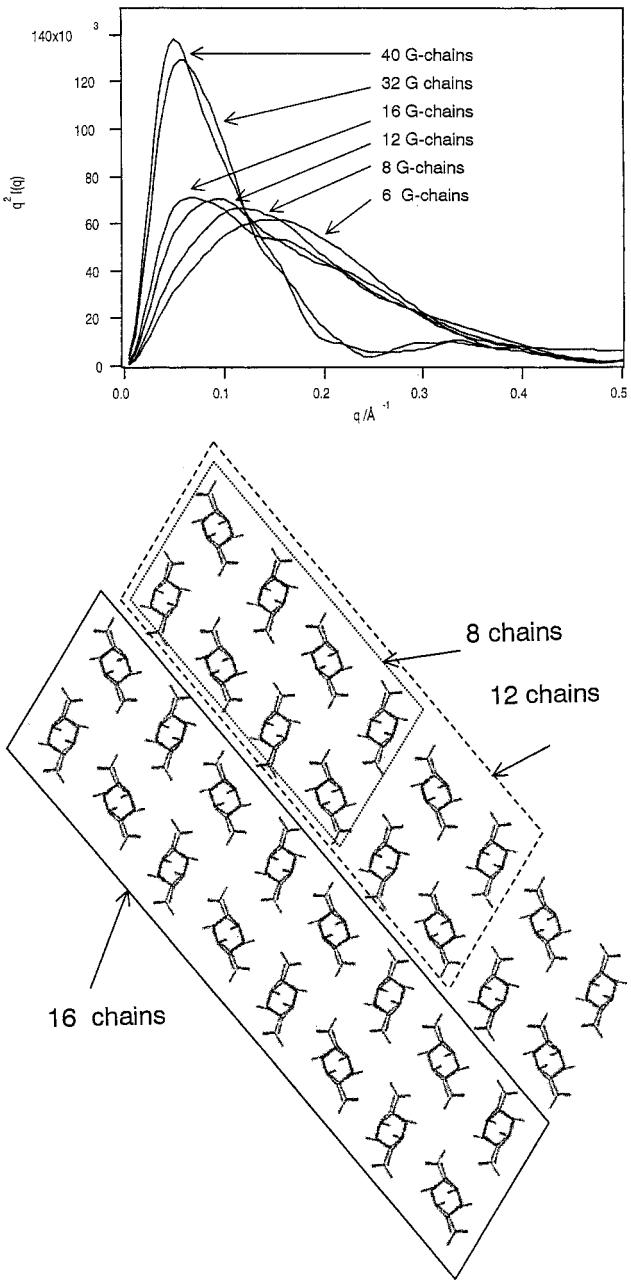

Figure 7. (Top) Scattering profiles calculated from the molecular models representing junction zones composed of a number of associated oligoguluronates (DP = 24). (Bottom) The corresponding molecular model projections.

where g_i and $\phi_i(q)$ denote the atomic scattering weight and the particle scattering factor of atom i and d_{ij} is the interatomic distance between atoms i and j. The atomic particle scattering factor is assumed to be identical to that of a rigid sphere with a radius equal to the van der Waals radius of the atom:

$$\phi_i(q) = 3\frac{\sin(R_i q) - (R_i q)\cos(R_i q)}{(R_i q)^3} \quad (4)$$

The model junction zones were derived from the reported X-ray fiber diffraction data of high-G alginates[9] assuming increasing degree of polymerization of homoguluronate and considering increasing number of laterally associated chains with a maximum of 40 chains (Figure 7). The detailed localization of the gel-inducing

Table 6. Parameters from Molecular Model Fits to SAXS Data from Ca−Alginate Gels Using $CaCO_3$ as the Ca^{2+} Source

alginate source	c_p (g/L)	$[Ca^{2+}]$ (mM)	single M-chain	aggregated G-chains	constant term
InG_{155}	5	7.5	4%	12 chains (96%)	4
	7.5	11.25	14%	12 chains (86%)	8
	10	7.5	42%	6 chains (58%)	0.5
	10	10	15%	8 chains (85%)	2
	10	15	6%	12 chains (94%)	1
	10	25	8%	32 chains (92%)	4
	12.5	18.5	3%	12 chains (97%)	1

Ca ions was not reported in that study. This indicates that the contribution to the electron density from the Ca^{2+} ions affects the average electron density of the junction zones more than a localized effect. Thus, the calculations were carried out by calculating the scattering from the junction zones only without an explicit representation of the Ca^{2+} ions. We selected a degree of polymerization DP = 24 for the oligoguluronate and assumed perfect matching in this calculations. The different distributions of DP of the oligoguluronate sequences in various alginates were not considered in these model calculations, but possible elaboration of the present approach is discussed below. Figure 7 shows such calculated data presented as the Kratky plots of laterally associated oligoguluronate chains of various degrees, along with the projection of the corresponding model junction zones. The estimated $R_{g,c}$ for the associated oligoguluronates using these models were found to be 4.0, 5.1, 5.6, and 8.3 Å for the duplex, triplex, quadruplex, and heptamer junction zones, respectively. Thus, the values of R_1 and R_2 evaluated from the two-component broken rod model indicate that a rather large number of chains are laterally associated side-by-side in the junction zones.

However, the model calculations using only one association mode at the time could not account for the coexistence of the junction zone multiplicity. The two-component broken rod model eq 2 was therefore modified to calculate a total scattering intensity for alginate gels using the molecular model as

$$I(q) = k_1\Theta_1(q) + k_2\Theta_2(q) + k_3/q^2 \qquad (5)$$

where $\Theta_i(q)$ is given by eq 3 for each of the components (association modes) included. Equation 5 implies that the gel is composed of two components having no spatial correlation. Although the alginate gel includes junction zones of different multiplicity, we have adopted a two-component approximation for the distribution of junction zone multiplicity and a single chain for computational simplicity. Thus, the estimated multiplicity will be considered as an average with respect to both the mode of packing and the number of chains involved. The mode of packing was chosen to fit the observed SAXS profiles. The analyzed results in terms of eq 5 are shown in Table 6 for InG_{155} in various conditions. The fitting example is shown in Figure 8 for the series of InG155 with the same $[Ca^{2+}]/c_p$ ratio in order to confirm that the constant $[Ca^{2+}]/c_p$ yields a similar ultrastructure at different c_p . The scattering profiles in Figure 8 are calculated assuming that the junction zones constitute 95% of the material and exist in 12-chain associates and 5% single chains rather than taking the best-fit parameters. This corresponds to the average results obtained for this series (Table 6).

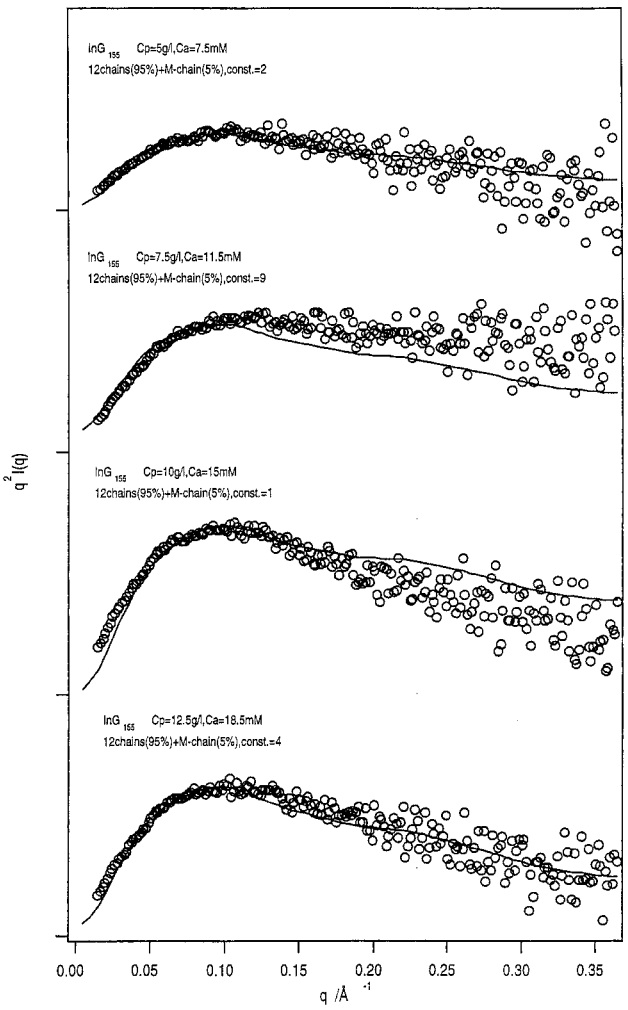

Figure 8. Kratky plots of SAXS data for alginate InG_{155} gels at constant ratio $c_p/[Ca^{2+}]$ and c_p from 5 to 12.5 mg/mL. The scattering profiles (solid lines) are calculated according to the modified broken rod model by assuming the systems composed of 95% 12 oligoguluronate (DP = 24) associated junction zones (Figure 7) and 5% single mannuronan chains (DP = 24).

Distance Distribution Functions. Direct inspection of the distance distribution function, $p(r)$, obtained by direct Fourier inversion of the scattering profiles applying the equation[35]

$$p(r) = (2\pi)^2 \int_0^\infty I(q)(qr)\,\sin(qr)\,\mathrm{d}q \qquad (6)$$

also bespeaks of representation of the junction zones in the model using more than one component. The distance distribution functions (Figure 9) show, in addition to the peak centered in the region r = 30 Å, a long tail with a clear shoulder in the region r = 100−200 Å for some of the gels. The distance distribution function for the alginate chains shows only one peak centered around r = 30 Å.[36] Note also that the $p(r)$ for the alginate gels are distinct from that of the gellan gels[40] by not showing any negative values of $p(r)$ corresponding to a correlation hole.

Syneresis. Syneresis of a gel is a phenomena that macroscopically is characterized by a slow, time-dependent deswelling of the gel and thereby partly expelling liquid. Little is known about the molecular mechanisms leading to this phenomenon in the alginate gels. Small-angle X-ray scattering was therefore observed from alginate gels in the syneretic domain of conditions;

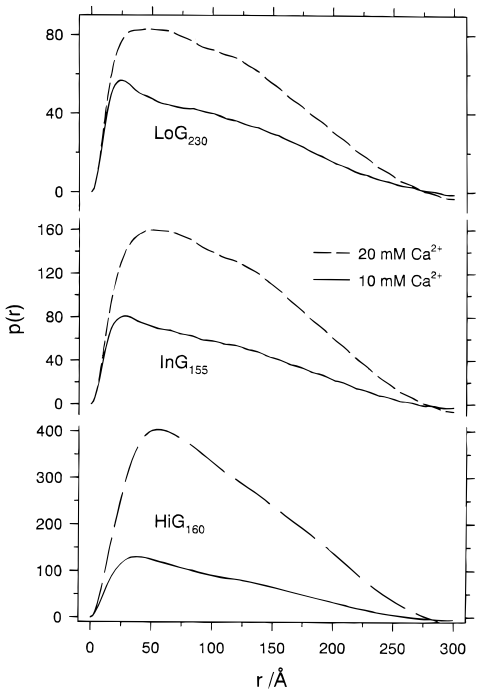

Figure 9. Distance distribution functions, $p(r)$, evaluated by Fourier transform of the SAXS data from 10 mg/mL homogeneous alginate LoG_{230}, InG_{155}, and HiG_{160} gels, using CaEGTA as the Ca^{2+} source for $[Ca^{2+}] = 10$ and 20 mM, respectively.

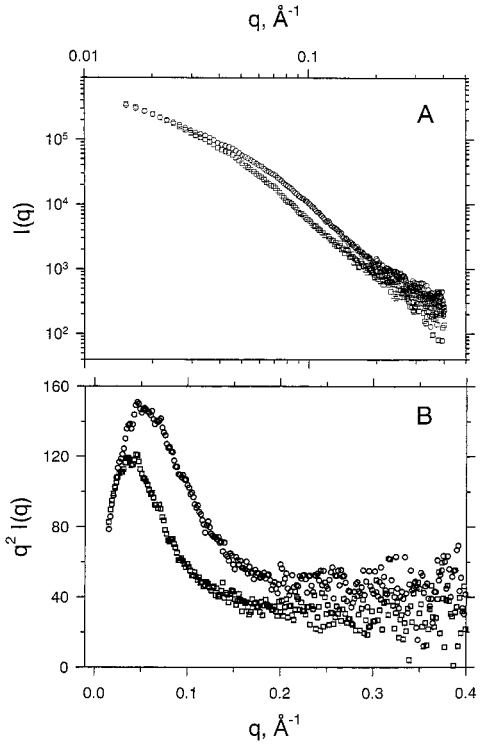

Figure 10. Double logarithmic (A) and Kratky plot (B) of SAXS data of homogeneous 10 mg/mL alginate HiG_{160} gels at $[Ca^{2+}] = 30$ mM using $CaCO_3$ (□) and CaEGTA (○) as the Ca source.

in particular, $[Ca^{2+}] = 30$ mM, and HiG_{160} alginate was selected. The SAXS profile of the gel after syneresis (Figure 10) shows a further increase in the cross-sectional radius (Tables 4 and 5). This indicates that further lateral association of junction zones contributes to syneresis in alginate gels. The kinetics of syneresis is slow compared to the kinetics of the gel cure experiments and may suggest that the junction zone association leading to the syneresis occurs when the elastic segments are far away from their equilibrium end-to-end distance. Becoming associated with a junction zone while the elastic segment is stretched, it may exert an elastic restoring force to the network, thereby leading to reduction of the overall volume of the network.

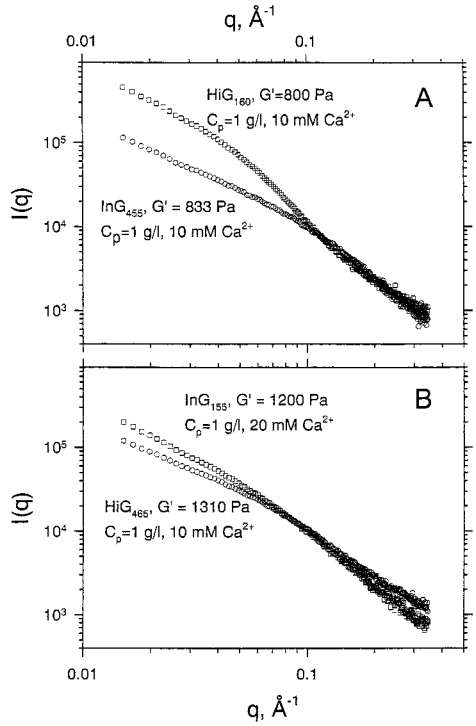

Figure 11. Comparison of scattering profiles for 10 mg/mL alginate gels having nearly the same G'. Alginate gels with $G' = 815 \pm 20$ Pa (A) obtained using alginate InG_{455} (○) and HiG_{160} (□), and both gels have $[Ca^{2+}] = 10$ mM using CaEGTA. Alginate gels with $G' = 1250 \pm 60$ Pa (b) using alginate from InG_{155}, $[Ca^{2+}] = 20$ mM (□), and HiG_{465}, $[Ca^{2+}] = 10$ mM (○) using CaEGTA.

Comparison of SAXS Data for Gels of Similar Storage Modulus. The rheological characterization shows that gels of similar storage modulus, G', for a given c_p can be obtained using different alginates and $[Ca^{2+}]$ combinations. It is of interest to compare the SAXS data of such "isoelastic" gels to explore any resemblance in local structure as well. Figure 11 compares the SAXS data for $c_p = 10$ mg/mL gels having G' equal to 815 Pa within 3% (a) and G' equal to 1250 Pa within 5% (b). The actual gels in the first comparison are made from InG_{455} and HiG_{160} alginates, and both gels have $[Ca^{2+}] = 10$ mM using CaEGTA (Figure 11a). The gels in the second comparison are InG_{455} alginate using $[Ca^{2+}] = 20$ mM from CaEGTA and HiG_{465} using $[Ca^{2+}] = 10$ mM also from CaEGTA (Figure 11b). The data show that there are significant differences in the scattering data for gels with similar G'. In the first example, the mass fractal dimensionality estimated from $\log(I(q))$ vs $\log(q)$ in the linear region around $q = 0.1$ Å^{-1} for the two gels are estimated as 2.05 (InG_{455}, $q \in (0.08-0.34)$ Å^{-1}) and 2.5 (HiG_{160}, $q \in (0.05-0.21)$ Å^{-1}). Similar large fractal dimensionality has previously been estimated for κ-carrageenan gels[41] and suggested to be consistent with junction zones formed by a two-step mechanism consisting of duplex formation and subsequent further association. Also for the gels compared at $G' = 1250 \pm 60$ Pa, there are differences; the two mass fractal dimensionalities are estimated as 1.9 (InG_{455}, $q \in (0.05-0.15)$ Å^{-1}) and 1.8 (HiG_{465}, $q \in (0.05-$

0.2) $Å^{-1}$). The additional evidence emerging from the SAXS data is that this is at least partly due to an increasing junction zone multiplicity. This suggests that gels with similar elasticity but with different local structure can be prepared by a suitable combination of alginate source, degree of polymerization, and gelling conditions. Or in other words, the mechanical strength and local structure of alginate gels can be varied independently within this family of polysaccharides. Recently, diffusional properties of bovine serum albumin (BSA) in alginate gel beads made from different sources have been reported.[42] These data suggest that diffusion of BSA is less restricted in gels made from alginates with large F_G, suggesting a more open character of the network formed by this type of alginate.

Concluding Remarks

This study shows that the formation of junction zones occurring on ionotropic gelation of alginate is readily monitored by small-angle X-ray scattering. The data show that homoguluronic acid sequences associate laterally to various multiplicities depending on the fractional Ca saturation of the guluronic acid, the alginate source, and the overall degree of polymerization. Lateral association of chain segments depends on several factors, including the formation of precursor structures, structural interruptions of regular residue sequences limiting the length of the junction zones, polymer chain segment concentration, and detailed packing geometry resulting in well-defined association numbers.

A molecular model describing this lateral association can be developed along the lines of an open association equilibrium model taking explicit account of total concentration of Ca^{2+}, alginate concentration, and the sequence distribution of the guluronic acid within the sample. Estimation of proper parameter values, in particular assignment of statistical weights for associations between G-sequences of polysaccharide chains already connected to the network, is a necessary prerequisite for such an approach. The guluronic acid sequence distribution for the various alginates imposes various structural interruptions limiting the maximum length of the junction zones in Ca^{2+}-induced gelation and is therefore an important additional factor that should be properly incorporated in the above-suggested molecular model. In a previous account of modeling the influence of sequence distribution on the alginate gelation properties, the second-order Markov model for sequence distribution was adopted.[43] This model was assumed because of the lack of an interpretation of the sequential triad data determined by NMR consistent with the biosynthesis of alginate. Recent progress in cloning the genes of the bacterial C-5 epimerase[44] opens up possibilities for improvements in elucidation of the sequential distribution of alginate. Refinement of the influence of alginate sequence on the ionotropic gelation, also in view of the SAXS data reported here, awaits further progress regarding the action pattern of the C-5 epimerases.

The results also show that the local structure of junction zones and the shear modulus can be controlled independently. This is one of several factors that should be considered when an alginate for a given application is selected. This study may therefore provide essential knowledge for an effective design of gel matrices of predetermined pore size and pore size distribution combined with various gel strengths, as is required for advanced uses of alginate gels.

Acknowledgment. Part of this work was performed under the approval of the Photon Factory Advisory Committee (Proposal No 94G 291). This work was supported by grants form Japan Society for Promotion of Science, the Ministry of Agriculture, Japan, the Minstry of Education, Science, Sports and Culture (Grant-in-aid 07455384), the Norwegian University of Science and Technology, NTNU, the Norwegian Research Council, and Pronova Biopolymers a.s., Drammen, Norway. The authours gratefully acknowledge the skillful assistance by engineer Ingrid Aune.

References and Notes

(1) Moe, S. T.; Draget, K. I.; Skjåk-Bræk, G.; Smidsrød, O. In *Food Polysaccharides and Their Applications*; Stephen, A., Ed.; Marcel Dekker: New York, 1995; p 245.
(2) Soon-Shiong, P.; Feldman, E.; Nelson, R.; Komtebedde, J.; Smidsrød, O.; Skjåk-Bræk, G.; Espevik, T.; Heintz, R.; Lee, M. *Transplantation* **1992**, *54*, 769.
(3) Soon-Shiong, P.; Feldman, E.; Nelson, R.; Heintz, R.; Yao, Q.; Yao, Z.; Zheng, T.; Merideth, N.; Skjåk-Bræk, G.; Espevik, T.; Smidsrød, O.; Sandford, P. *Proc. Natl. Acad. Sci. U.S.A.* **1993**, *90*, 5843.
(4) Soon-Shiong, P.; Heintz, R. E.; Merideth, N.; Yao, Q. X.; Yao, Z.; Zheng, T.; Murphy, M.; Moloney, M. K.; Schmehl, M.; Harris, M.; Mendez, R.; Mendez, R.; Sandford, P. A. *Lancet* **1994**, *343*, 950.
(5) Thu, B.; Bruheim, P.; Espevik, T.; Smidsrød, O.; Soon-Shiong, P.; Skjåk-Bræk, G. *Biomaterials* **1996**, *17*, 1069.
(6) Kulseng, B.; Thu, B.; Espevik, T.; Skjåk-Bræk, G. *Cell Transplantation* **1997**, *6*, 387.
(7) Grant, G. T.; Morris, E. R.; Rees, D. A.;. Smith, P. J. C.; Thom, D. *FEBS Lett.* **1973,** *32*, 195.
(8) Morris, E. R.; Rees, D.A.; Thom, D.; Boyd, J. *Carbohydr. Res.* **1978,** *66*, 145.
(9) Atkins, E. D. T.; Nieduszynski, I. A.; Mackie, W.; Parker, K. D.; Smolko, E. E. *Biopolymers* **1973**, *12*, 1865.
(10) Atkins, E. D. T.; Nieduszynski, I. A.; Mackie, W.; Parker, K. D.; Smolko, E. E. *Biopolymers* **1973**, *12*, 1879.
(11) Kohn, R. *Pure Appl. Chem.* **1975**, *42*, 371.
(12) Smidsrød, O.; Haug, A. *Acta Chem. Scand.* **1968**, *22*, 1989.
(13) Haug, A.; Smidsrød, O. *Acta Chem. Scand.* **1970**, *24*, 843.
(14) Thom, D.; Grant, G. T.; Morris, E. R.; Rees, D. A. *Carbohydr. Res.* **1982**, *100*, 29.
(15) Smidsrød, O. *J. Chem. Soc., Faraday Trans. 1* **1974**, *57*, 263.
(16) Mackie, W.; Perez, S.; Rizzo, R.; Vignon, M. *Int. J. Biol. Macromol.* **1983**, *5*, 329.
(17) Steginsky, C. A.; Beale, J. M.; Floss, H. G.; Mayer, R. M. *Carbohydr. Res.* **1992**, *225*, 11.
(18) Chandrasekaran, R.; Puigjaner, L. C.; Joyce, K. L.; Arnott, S. *Carbohydr. Res.* **1988**, *181*, 23.
(19) Chandrasekaran, R.; Radha, A.; Thailambal, V. G. *Carbohydr. Res.* **1992**, *224*, 1.
(20) Wang, Z.-Y.; White, J. W.; Konno, M.; Saito, S.; Nozawa, T. *Biopolymers* **1995**, *35*, 227.
(21) Skjåk-Bræk, G.; Grasdalen, H.; Smidsrød, O. *Carbohydr. Polym.* **1989,** *10*, 31.
(22) Mikkelsen, A.; Elgsaeter, A. *Biopolymers* **1995**, *36*, 17.
(23) Thu, B.; Skjåk-Bræk, G.; Micali, F.; Vittur, F.; Rizzo, R. *Carbohydr. Res.* **1997**, *297*, 101.
(24) Grasdalen, H. *Carbohydr. Res.* **1983**, *118*, 255.
(25) Christensen, B. E., personal communication.
(26) Draget, K. I.; Østgaard, K.; Smidsrød, O. *Carbohydr. Polym.* **1991**, *14*, 159.
(27) Ueki, T.; Hiragi, Y.; Izumi, Y.; Tagawa, H.; Kataoka, M.; Muroga, Y.; Matsushita, T.; Amemiya, Y. *Photon Factory Activity Report* **1983**, *1*, V7, V29, V170.
(28) Mimura, M.; Kitamura, S.; Gotoh, S.; Takeo, K.; Urakawa, H.; Kajiwara, K. *Carbohydr. Res.* **1996**, *289*, 25.
(29) Yuguchi, Y.; Urakawa, H.; Kajiwara, K.; Draget, K. I.; Stokke, B. T., submitted for publication.
(30) Skjåk-Bræk, G.; Smidsrød, O.; Larsen, B. *Int. J. Biol. Macromol.* **1986**, *8*, 330.
(31) Draget, K.; Simensen, M. K.; Onsøyen, E.; Smidsrød, O. *Hydrobiologia* **1993**, *260/261*, 563.

(32) Almdal, K.; Dyre, J.; Hvidt, S.; Kramer, O. *Polym. Gels Networks* **1993**, *1*, 5.
(33) Mikkelsen, A.; Elgsaeter, A. *Biopolymers* **1995**, *36*, 17.
(34) Thu, B.; Gåserød, O.; Paus, D.; Mikkelsen, A.; Skjåk-Bræk, G.; Toffanin, R.; Vittur, F.; Rizzo, R. *Biopolymers* **2000**, *53*, in press.
(35) Glatter, O.; Kratky, O. *Small-Angle X-ray Scattering;* Academic Press: London, 1982.
(36) Mimura, M.; Urakawa, H.; Kajiwara, K.; Draget, K. I.; Stokke, B. T., manuscript in preparation.
(37) Guenet, J.-M. *Thermoreversible Gelation of Polymers and Biopolymers*; Academic Press: London, 1992; pp 89−186.
(38) Burchard, W.; Michel, E.; Trappe, V. *Macromolecules* **1996**, *29*, 5934.
(39) Glatter, O. *Acta Phys. Aust.* **1980**, *52*, 243.
(40) Yuguchi, Y.; Mimura, M.; Kitamura, S.; Urakawa, H.; Kajiwara, K. *Food Hydrocolloids* **1993**, *7*, 373.
(41) Kajiwara, K.; Kohjiya, S.; Shibayama, M.; Urakawa, H. In *Polymer Gels; Fundamentals and Biomedical Applications;* DeRossi, D., Kajiwara, K., Osada, Y., Yamauchi, A., Eds.; Plenum Press: New York, 1991; p 3.
(42) Marthinsen, A.; Storrø, I.; Skjåk-Bræk, G. *Biotechnol. Bioeng.* **1992**, 186.
(43) Stokke, B. T.; Smidsrød, O.; Bruheim, P.; Skjåk-Bræk, G. *Macromolecules* **1991**, *24*, 4637.
(44) Ertesvåg, H.; Høidal, H. K.; Hals, I. K.; Rian, A.; Doseth, B.; Valla, S. *Mol. Microbiol.* **1995**, *16*, 719.

MA991559Q